Lithos 170–171 (2013) 105–116

Contents lists available at SciVerse ScienceDirect

Lithos

journal homepage: www.elsevier.com/locate/lithos

Geochemistry and petrogenesis of Mashhad granitoids: An insight into the geodynamic history of the Paleo-Tethys in northeast of Iran

H. Mirnejad [a,*], A.E. Lalonde [b,1], M. Obeid [c], J. Hassanzadeh [d]

[a] Department of Geology, Faculty of Science, University of Tehran, Tehran 14155-64155, Iran
[b] Department of Earth Sciences and Ottawa-Carleton Geoscience Centre, University of Ottawa, Ottawa, Ontario, Canada
[c] Geology Department, Faculty of Science, Fayoum University, Fayoum, Egypt
[d] Division of Geological and Planetary Sciences, California Institute of Technology, Pasadena, CA 91125, USA

ARTICLE INFO

Article history:
Received 5 July 2012
Accepted 3 March 2013
Available online 15 March 2013

Keywords:
Granitoid
Paleo-Tethys
Geodynamic history
Mashhad
Iran

ABSTRACT

Mashhad granitoids in northeast Iran are part of the so-called Silk Road arc that extended for 8300 km along the entire southern margin of Eurasia from North China to Europe and formed as the result of a north-dipping subduction of the Paleo-Tethys. The exact timing of the final coalescence of the Iran and Turan plates in the Silk Road arc is poorly constrained and thus the study of the Mashhad granitoids provides valuable information on the geodynamic history of the Paleo-Tethys. Three distinct granitoid suites are developed in space and time (ca. 217–200 Ma) during evolution of the Paleo-Tethys in the Mashhad area. They are: 1) the quartz diorite–tonalite–granodiorite, 2) the granodiorite, and 3) the monzogranite. Quartz diorite–tonalite–granodiorite stock from Dehnow–Vakilabad (217 ± 4–215 ± 4 Ma) intruded the pre-Late Triassic metamorphosed rocks. Large granodiorite and monzogranite intrusions, comprising the Mashhad batholith, were emplaced at 212 ± 5.2 Ma and 199.8 ± 3.7 Ma, respectively. The high initial $^{87}Sr/^{86}Sr$ ratios (0.708042–0.708368), low initial $^{143}Nd/^{144}Nd$ ratios (0.512044–0.51078) and low $\varepsilon_{Nd(t)}$ values (−5.5 to −6.1) of quartz diorite–tonalite–granodiorite stock along with its metaluminous to mildly peraluminous character ($Al_2O_3/(CaO + Na_2O + K_2O)$ Mol. = 0.94–1.15) is consistent with geochemical features of I-type granitoid magma. This magma was derived from a mafic mantle source that was enriched by subducted slab materials. The granodiorite suite has low contents of Y (≤18 ppm) and heavy REE (HREE) (Yb < 1.53 ppm) and high contents of Sr (>594 ppm) and high ratio of Sr/Y (>35) that resemble geochemical characteristics of adakite intrusions. The metaluminous to mildly peraluminous nature of granodiorite from Mashhad batholiths as well as its initial $^{87}Sr/^{86}Sr$ ratios (0.705469–0.706356), initial $^{143}Nd/^{144}Nd$ ratios (0.512204–0.512225) and $\varepsilon_{Nd(t)}$ values (−2.7 to −3.2) are typical of adakitic magmas generated by partial melting of a subducted slab. These magmas were then hybridized in the mantle wedge with peridotite melt. The quartz diorite–tonalite–granodiorite stock and granodiorite batholith could be considered as arc-related granitoid intrusions, which were emplaced during the northward subduction of Paleo-Tethys Ocean crust beneath the Turan micro-continent. The monzogranite is strongly peraluminous ($Al_2O_3/(CaO + Na_2O + K_2O)$ Mol. = 1.07–1.17), alkali-rich with normative corundum ranging between 1.19% and 2.37%, has high initial $^{87}Sr/^{86}Sr$ ratios (0.707457–0.709710) and low initial $^{143}Nd/^{144}Nd$ ratios (0.512042–0.512111) and $\varepsilon_{Nd(t)}$ values (−5.3 to −6.6) that substantiate with geochemical attributes of S-type granites formed by dehydration-melting of heterogeneous metasedimentary assemblages in thickened lower continental crust. The monzogranite was emplaced as a consequence of high-temperature metamorphism during the final integration of Turan and Iran plates. The ages found in the Mashhad granites show that the subduction of Paleo-Tethys under the Turan plate that led to the generation of arc-related Mashhad granites in late-Triassic, finally ceased due to the collision of Iran and Turan micro-plates in early Jurassic.

1. Introduction

The basement of Iran, which was consolidated in late Precambrian as the result of Pan-African orogeny, is composed principally of metamorphic rocks and in part granites. This basement was, however, fragmented and rifted from Gondwana as the Paleo-Tethys and Neo-Tethys oceans opened and later re-combined (Berberian and King, 1981; Şengör, 1987). These important tectonic events affected the Iranian and adjacent plates, including the African, Indian, Arabian, and Eurasian plates, during Cambrian to Tertiary times (Alsharhan et al., 2001). The Tethyan region, which comprises the Iranian plate and adjacent areas, was subjected to three major evolutionary stages. The

* Corresponding author. Tel./fax: +98 21 6111 2959.
E-mail address: mirnejad@khayam.ut.ac.ir (H. Mirnejad).
[1] Deceased (December, 2012).

0024-4937/$ – see front matter © 2013 Elsevier B.V. All rights reserved.
http://dx.doi.org/10.1016/j.lithos.2013.03.003

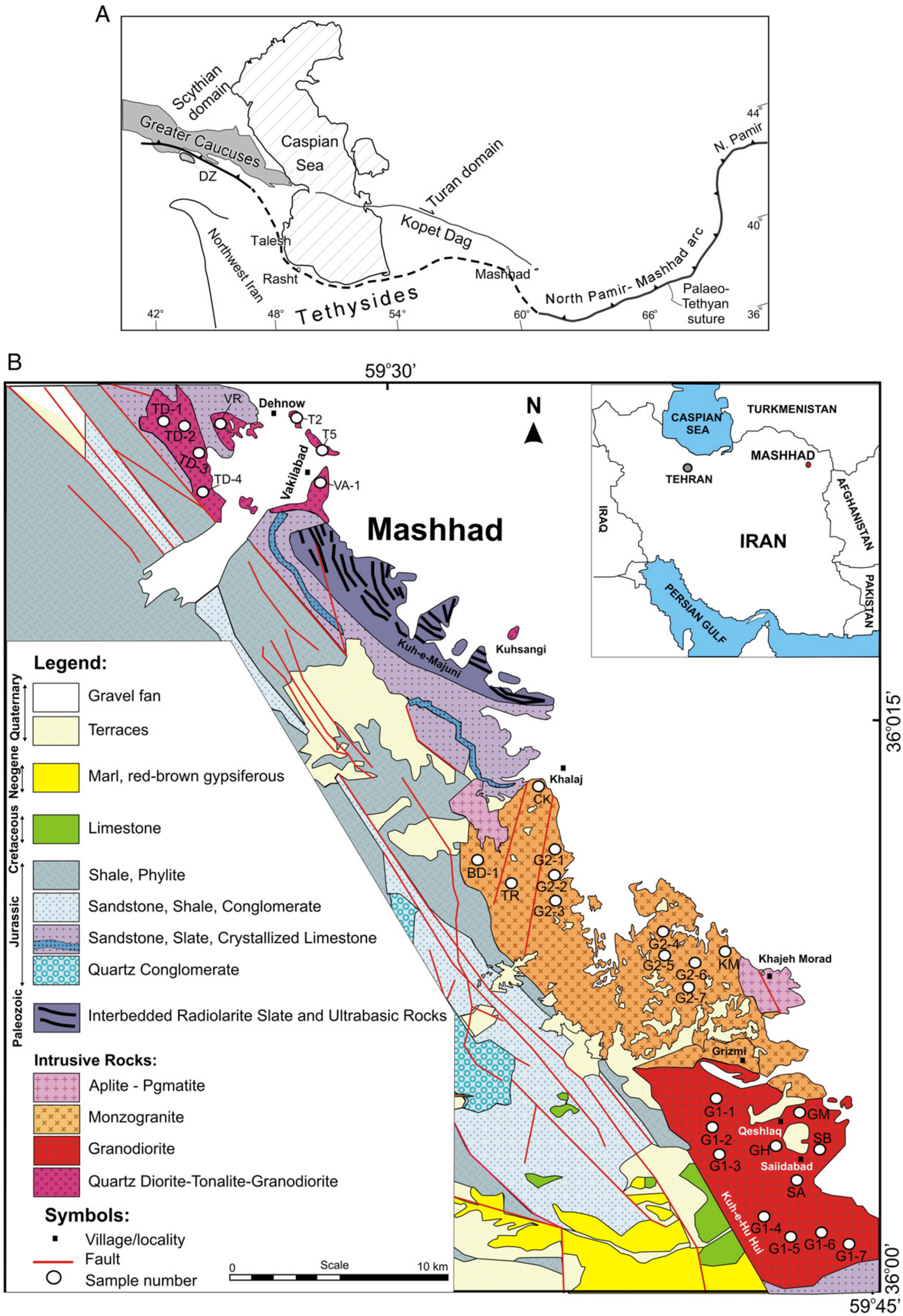

Fig. 1. (A) The North Pamir–Mashhad arc that passes south of Mashhad city and marks the Paleo-Tethys suture zone. (B) Geological map of Mashhad. Inset is the map of Iran showing the position of Mashhad city.
Panel A is after Natal'in and Şengör (2005). Panel B is from the Geological Survey of Iran (1984).

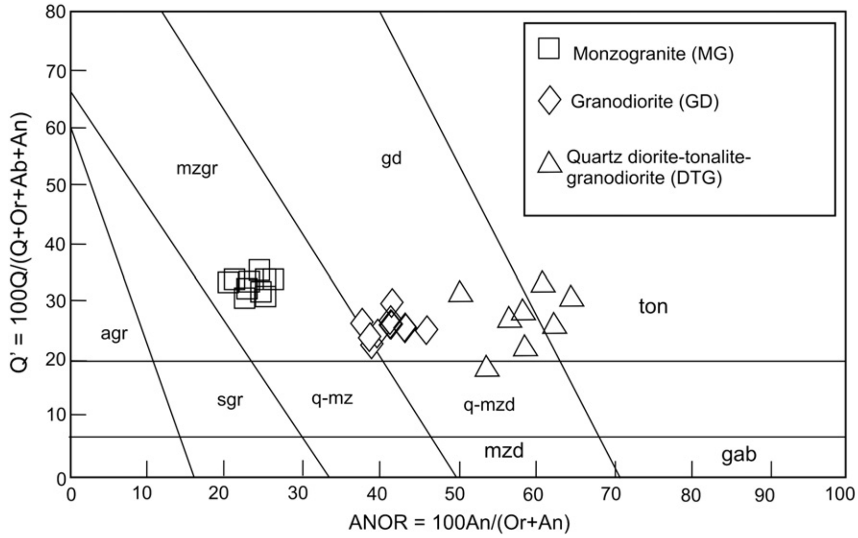

Fig. 2. Normative compositions of Mashhad granitoid suites in the Q′ANOR diagram of Streckeisen and Le Maitre (1979). Normative fields: agr: alkali feldspar granite, sgr: syenogranite, mzgr:monzogranite, gd: granodiorite, ton: tonalite, q-mz: quartz monzonite, q-mzd: quartz monzodiorite, mzd: monzodiorite, and gab:gabbro.

first of these was the closing of the Paleo-Tethys and rifting of the Neo-Tethys from early Permian to late Triassic times. The second stage saw the onset of subduction of the Neo-Tethys and the collision of the Indian plate with the Eurasian plate from the Jurassic to the early Lower Tertiary. The third and last stage was marked by the collision of the Arabian plate with the Eurasian plate from early Tertiary to the present.

The northward subduction of Paleo-Tethys during the late Palaeozoic–early Mesozoic created a magmatic arc, called Silk Road arc, at the southern margin of Eurasia. According to Natal'in and Şengör (2005), the oblique subduction and longitudinal shortening of Paleo-Tethys fragmented the Silk Road arc by arc-shaving and slicing strike slip faults and thus the Paleo-Tethyan suture zone is incomplete in some areas. In Iran, the only well-exposed lithologies within the Paleo-Tethys suture zone are found at the west end of the Mashhad–North Pamir arc and in the vicinity of Mashhad city (Fig. 1A). These include some fragments of ophiolites south of the city, a 5 × 25 km granitic batholith in the south–southeast and a granitic stock in the northwest (Fig. 1B). Dating by the $^{40}Ar/^{39}Ar$ method of the ophiolite complex has yielded plateau ages of 281–277 Ma (Ghazi et al., 2001) which indicate that obduction and thus emplacement of the Paleo-Tethys remnants occurred during the Early Permian. However, contradictory data exists on the exact timing of granite crystallization, many of which are not supported by stratigraphic ages. For example, Majidi (1978) reported K–Ar ages of 350–210 Ma, while Alberti et al (1973) obtained younger K–Ar ages in the range of 120–145 Ma. On the contrary, field observations indicate that the Mashhad granites had intruded the ophiolite complex and are in turn overlain unconformably by the basal conglomerates of lower Jurassic (Hashemi, 2004). The granites must therefore have been emplaced by early Jurassic. Karimpour et al. (2010a) obtained 215–217 Ma U–Pb zircon ages for the isolated and small quartz diorite–tonalite–granodiorite bodies that outcrop in the Dehnow–Vakilabad regions, located ~10 km to the northwest of the Mashhad batholith. Although such age determination is more consistent with the cross-cutting relations observed in the region, the other U–Pb zircon ages reported by Karimpour et al. (2010b, 2011) from the main Mashhad batholith (i.e., 205.9 ± 4.1 Ma and 201 ± 3.7 Ma for the collision- and arc-related granitoids, respectively) contradict field observations, nor are they supported by the geodynamic history of Paleo-Tethys in northeast Iran. In addition, models suggested so far for the source of Mashhad granites (e.g. metaplate–metapsmatite, meta-graywacke, etc.) contradict their geochemical characteristics and need re-examination. It is therefore imperative to report new geochemical data and age determinations for granitoids from the Mashhad batholith.

Granitoid rocks display great diversity in their origin, source and petrogenesis and thus can be used as indicators of geodynamic environments and, in some cases, as tracers of geodynamic evolution (Barbarin, 1999). In this paper we present field relationships and new geochemical–geochronological data on granitoids from Mashhad in order to constrain the exact timing of their emplacement, the likely tectonic setting during their formation and their ultimate sources. This study also provides important clues on the geodynamic history of the Paleo-Tethys, by estimating the timing and duration of its subduction and closure in NE Iran.

2. Geological setting

The Mashhad granitoids, located at 59°22′–59°45′N, 36°00′–36°22′E and in the northeastern slopes of Binalood Mountains, cover an area of about 700 km^2 (Fig. 1B). They are situated within the Paleo-Tethys remnants consisting of structurally deformed ophiolites and low- to medium-grade metamorphosed rocks. This assemblage resulted from the obduction of the Paleo-Tethys oceanic crust over the Iranian microcontinental margin during terrane accretion (Alavi, 1991; Stöcklin, 1974). The ophiolites are surrounded by metamorphic rocks, including well-layered slate, phyllite, schist, marble, and carbonate meta-conglomerate of Permian age (Razavi et al., 2008). Alavi (1979, 1991) reconstructed the original sedimentary environment and its depositional setting for these metamorphic rocks and considered the entire assemblage indicative of deposition in deep water settings such as turbidite deposits which formed in a trench–forearc basin over a north-dipping subduction zone.

Based on their topographic expression and field observations, the granitoid rocks of Mashhad occur in a large batholith to the south–southeast of Mashhad and also a smaller isolated stock to the northwest of the city (Fig. 1B). Field relationships show that these lithologies were emplaced in various stages and over a long time span, before the intrusion of pegmatite–aplite dykes.

3. Petrography

The petrographic study is based on 60 samples collected from all three granitoid suites. Considering the modal abundances of minerals, the Mashhad granitic rocks are classified as (1) quartz diorite–tonalite–granodiorite (DTG), (2) granodiorite (GD), and

(3) monzogranite (MG). This nomenclature is also supported by the normative composition (Fig. 2).

The DTG suite, which comprises the Dehnow–Vakliabad stock in NW of Mashhad city, is composed mainly of plagioclase, quartz, biotite and accessory minerals which include K-feldspar, amphibole, zircon, apatite and epidote. Plagioclase (3 mm across) is subhedral to anhedral and shows optical zonation. Quartz (0.8 mm across) is anhedral and occurs as aggregates of smaller grains. Biotite forms equant flakes, sometimes intergrown with amphibole and contains inclusions of apatite, zircon and titanite.

The GD suite, cropping out in the southeast part of the Mashhad batholith, consists of feldspar, quartz and mica as main mineral phases and zircon, apatite, allanite and titanite as accessory phases. Plagioclase is subhedral to anhedral, has an average size of 4.5 mm and occasionally contains anhedral xenocrysts of quartz and biotite. Quartz (2 mm) is anhedral, has undulatory extinction and sometimes has inclusions of apatite and rutile. K-feldspar (0.4 mm) is microcline and orthoclase and shows both Carlsbad and grid-twinning in thin sections. In some places, this mineral forms large phenocrysts that can reach up to 6 mm in diameter. Biotite is subhedral to anhedral and contains prismatic grains of apatite and zircon. It can also form interstitial grains between other minerals, and inclusions in feldspar.

The MG suite, occurs along the northwestern portion of the Mashhad batholith, is composed of quartz, plagioclase, K-feldspar, biotite and muscovite, with apatite and zircon as accessory minerals. Quartz (3 mm), the most abundant mineral, occasionally has inclusions of K-feldspar, biotite and plagioclase. K-feldspar (1.5 mm) is euhedral to subhedral, has inclusions of quartz and plagioclase, and in places shows alteration to kaolinite. Plagioclase (2 mm) is euhedral to subhedral, shows polysynthetic twining and has developed myrmekitic intergrowths at its contacts with quartz grains. Biotite (1 mm) with inclusions of zircon and apatite is sometimes altered to chlorite. Muscovite (0.5 mm) is euhedral to subhedral and occurs as either discrete grains or intergrowths with biotite.

4. Analytical techniques

Out of 60 samples collected from outcrops of unaltered Mashhad granitoids, the freshest specimens were initially examined by polarized light microscopy and selected for geochemical and isotopic analyses. Samples were crushed and powdered to 200 mesh in an agate mill. Major and trace element contents were determined by inductively coupled plasma-optical emission spectroscopy (ICP-OES) and inductively coupled plasma-mass spectrometry (ICP-MS), respectively, at Geosciences Laboratories in Sudbury, Canada. All samples for ICP analyses were dissolved using an alkali fusion ($LiBO_2$/$Li_2B_4O_7$) method. The analytical precision and accuracy are generally better than 5% for most elements. Radiogenic isotopic analyses were performed on whole-rock powders, digested in closed Savillex beakers using ultrapure HF and HNO_3 in a proportion of 2:5 and heated for 48 h to ensure complete digestion. The elements Rb, Sr, REE and Pb were separated using ion-exchange chromatography (see Cousens et al., 2003). The average values of total procedural blanks obtained during the time that this work was done are as follow: Rb 0.5 ng, Sr 1.5 ng, Sm 0.04 ng and Nd 0.26 ng. Strontium and Nd isotope ratios were measured on a Triton mass spectrometer at Carleton University, operated in the static mode. On the basis of numerous runs collected during the course of this work, average values (and respective 2σ uncertainties) for the isotopic ratios of the following standards were: NBS-987 $^{87}Sr/^{86}Sr = 0.710251 \pm 0.000020$ and La Jolla $^{143}Nd/^{144}Nd = 0.511870 \pm 0.000020$. Measured Sr and Nd isotope ratios for unspiked samples were corrected for fractionation using $^{88}Sr/^{86}Sr = 8.3752$ and $^{146}Nd/^{144}Nd = 0.7219$.

Our zircon U–Pb age determination is based on U, Pb, and Th isotopic measurements employing spot analysis using the Cameca IMS 1270 ion microprobe at the University of California, Los Angeles (UCLA). Analytical methods follow the procedures described by Quidelleur et al. (1997) and Schmitt et al. (2003a, 2003b). Zircon grains were first separated by conventional liquid and magnetic techniques, then hand selected under the binocular microscope, mounted in epoxy, and coated with ~100 Å of gold. The ion-microprobe spot analyses utilized a primary ion beam focused to a ~30 μm diameter spot and a secondary ion beam with a mass resolving power of 5000 amu and energy window of 50 eV. Following a pre-sputtering period of ~180 s, each analysis collected data for 8–10 cycles. The sample chamber was flooded with oxygen at $\sim 3 \times 10^{-5}$ Torr to enhance secondary Pb^+ ionization. The reported weighted-mean ages are based on $^{206}Pb/^{238}U$ ages calculated using the zircon standard AS3 (1099 ± 0.5 Ma; Paces and Miller, 1993). Common lead corrections were made using the measured values of ^{204}Pb (Stacey and Kramers, 1975) and the values of ^{208}Pb corrected for ^{232}Th-derived ^{208}Pb (Compston et al., 1984), which are considered a proxy for common ^{206}Pb and ^{207}Pb. These corrections use the anthropogenic Pb compositions reported for the Los Angeles basin (Sañudo-Wilhelmy and Flegal, 1994). ISOPLOT (Ludwig, 2003) was used for age calculations and plotting.

5. Geochemistry

The DTG stock of the Dehnow–Vakilabad area has a wide range of major and trace element contents (Table 1). The suite ranges in its SiO_2 contents from 60 to 65 wt.% and is thus intermediate in composition. It also has lower $Na_2O + K_2O$, Rb/Sr, Rb, Nb and higher MgO, FeOt, CaO and TiO_2 compared with the GD and MG (Table 1). The DTG

Table 1
Major oxide (wt.%) and trace element (ppm) contents of Mashhad granitoid rocks.

	DTG suite		GD suite		MG suite	
Sample no.	VA-1	VR	GH	SB	BD-1	CK
SiO_2	64.01	60.31	65.52	67.29	72.15	72.84
TiO_2	0.48	0.69	0.51	0.56	0.16	0.15
Al_2O_3	16.92	17.45	16.23	14.98	14.53	14.64
Fe_2O_3t	5.17	6.68	3.45	3.96	1.10	1.21
MnO	0.11	0.13	0.06	0.10	0.04	0.07
MgO	1.32	2.20	1.29	1.23	0.26	0.24
CaO	4.64	5.10	3.23	3.02	1.08	1.00
Na_2O	2.72	2.55	3.69	3.34	3.29	3.45
K_2O	2.91	2.91	4.05	3.98	5.03	5.01
P_2O_5	0.17	0.21	0.28	0.21	0.14	0.14
L.O.I.	1.44	1.82	1.32	1.23	0.96	1.06
Total	99.89	100.06	99.62	99.90	98.74	99.81
Ba	574	597	1457	1121	415	388
Cr	54	35	58	61	48	45
Nb	32	22	39	42	26	26
Ni	4	4	6	6	2	2
Rb	120	113	152	189	283	301
Sr	420	540	1234	701	186	197
Ta	2	2	3	3	2	2
Th	14	12	26	24	12	15
U	2	1	3	3	4	5
V	28	70	56	60	6	4
Y	15	22	14	15	8	10
Zr	178	154	217	197	76	89
La	43.53	41.59	94.63	78.23	27.87	29.33
Ce	88.87	83.42	159.21	131.45	52.88	62.12
Pr	9.37	9.20	15.03	12.27	5.16	6.57
Nd	34.58	33.91	48.30	39.81	17.62	19.87
Sm	6.09	6.19	6.77	5.57	3.57	4.33
Eu	1.50	1.61	1.58	1.34	0.65	0.81
Gd	4.39	4.98	4.10	4.01	2.74	2.97
Tb	0.58	0.72	0.51	0.61	0.39	0.40
Dy	2.99	4.06	2.63	2.91	1.78	1.82
Ho	0.52	0.79	0.48	0.51	0.27	0.31
Er	1.38	2.24	1.29	1.32	0.64	0.69
Tm	0.19	0.33	0.19	0.19	0.08	0.09
Yb	1.19	2.09	1.28	1.04	0.47	0.51
Lu	0.17	0.31	0.18	0.15	0.06	0.06

DTG = Quartz diorite–tonalite–granodiorite; GD = granodiorite; and MD = monzogranite.

constitutes a common suite with the GD on the basis of Harker variation diagrams (Fig. 3). Variation in major and trace elements with fractionation as recorded by increasing SiO_2 for the DTG rocks is depicted in Fig. 3. MgO, CaO, FeOt and Sr all show a marked decrease, while K_2O and Rb exhibit a slight increase with increasing SiO_2. The noticeable decline of MgO, CaO and FeOt reflects the early separation of amphibole, plagioclase and Fe–Ti oxides during crystallization of the DTG suite. The GD suite of the Mashhad batholith exhibits lower abundance of all major oxides, except Na_2O and K_2O contents, than those of the DTG suite (Table 1). The MG suite of the Mashhad batholith shows a restricted range in terms of major and trace element concentrations (Table 1). The suite has low MgO (0.08–0.31 wt.%), CaO (0.83–1.31 wt.%), Sr (131–244 ppm) and Y (8–20 ppm) and high Na_2O (3.17–3.74 wt.%), K_2O (4.79–5.24 wt.%), Rb (250–325 ppm) abundances. The MG suite does not show any definite trend in the Harker diagrams (Fig. 3). However, it is enriched in SiO_2 (72.15–73.64 wt.%) and depleted in MgO, FeOt, CaO, P_2O_5, Sr, V, Y and Zr relative to both the DTG and GR suites.

The non-alkaline nature of all three suites (DTG, GD and MG) is confirmed by the diagram of Sylvester (1989) (Fig. 4A), which discriminates between alkaline, calc-alkaline and highly fractionated calc-alkaline granites. In this diagram, all three suites fall in the calc-alkaline field, but the MG plots in the highly fractionated calc-alkaline field as delineated by its higher SiO_2 contents relative to the two other granitic suites. On the K_2O–SiO_2 diagram of Rickwood (1989) (Fig. 4B), the DTG suite plots in the medium-K calc-alkaline field whereas the GD samples straddle the medium-K and high-K calc-alkaline field (Fig. 4B). The aluminum saturation index [mol. Al_2O_3/($CaO + Na_2O + K_2O$)] (A/CNK) of Zen (1986) is plotted versus SiO_2 for the different granitoid suites (Fig. 4C). In this diagram, most of the DTG and GD analyses have metaluminous to mildly peraluminous affinities whereas the MG is mildly metaluminous to strongly peraluminous.

Chondrite-normalized REE plots of the DTG, GD and MG suites are shown in Fig. 5A. The REE patterns for three suites are very similar and characterized by LREE-enrichment, plus nearly absent or slightly negative Eu anomalies [$(Eu/Eu^*)_n = (0.59–0.95)$; average = 0.79] and pronounced fractionation [$(La/Yb)_n = 11.30–57.72$]. The DTG and GD show moderately LREE fractionated patterns [$(La/Sm)_n = 4.71–9.83$] and less fractionated HREE [$(Gd/Yb)_n = 1.27–2.04$]. The MG suite rocks, on the other hand, exhibit smooth inclined LREE patterns [$(La/Sm)_n = 4–5.87$] with moderately fractionated HREE [$(Gd/Yb)_n = 1.92–4.69$].

In the primitive mantle-normalized spider diagram (Fig. 5B), all three granitoid suites from Mashhad show enrichments in most of the large ion lithophile elements (LILE) and a fairly regular decrease towards high field strength elements (HFSE). The three suites also have pronounced negative Nb anomalies. The DTG suite has normalized patterns fairly similar to the GD, but the latter has generally higher LILE (Rb, Ba, K and Sr). The primitive mantle-normalized trace element

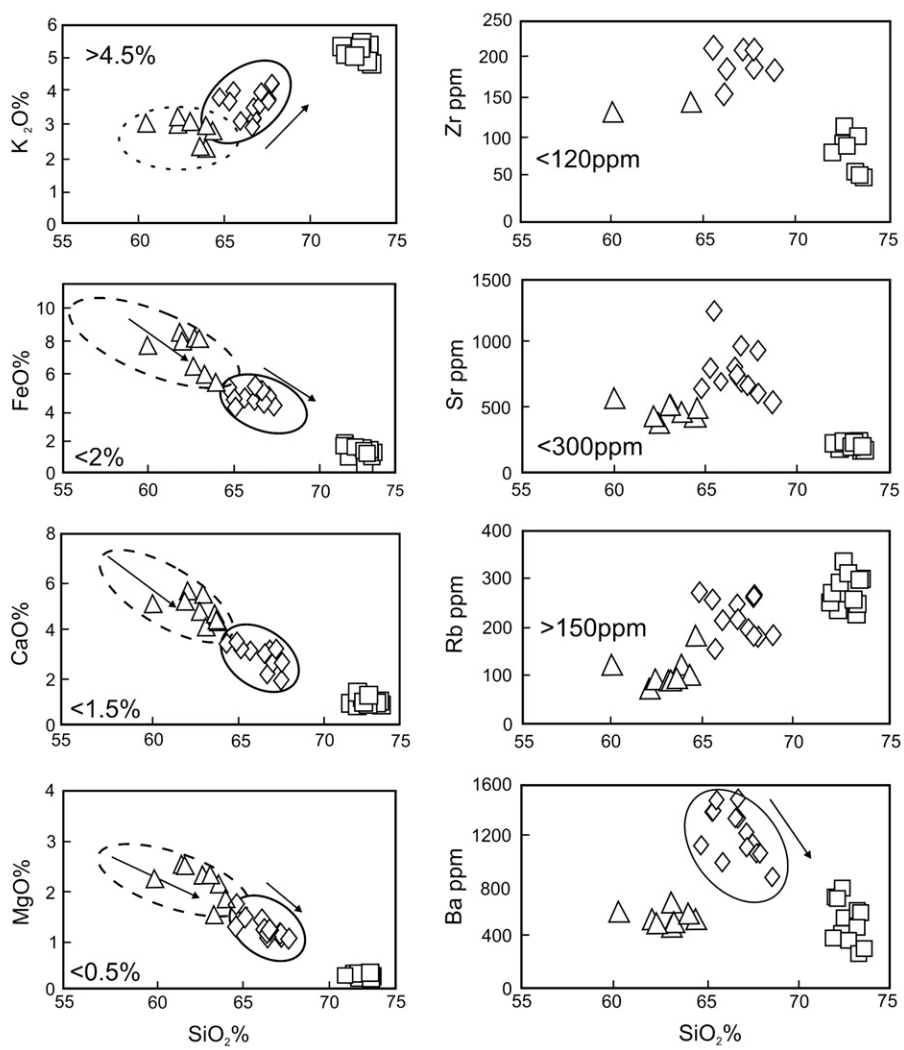

Fig. 3. Harker variation diagrams for some major and trace element compositions of Mashhad granitoid samples. Symbols as in Fig. 2.

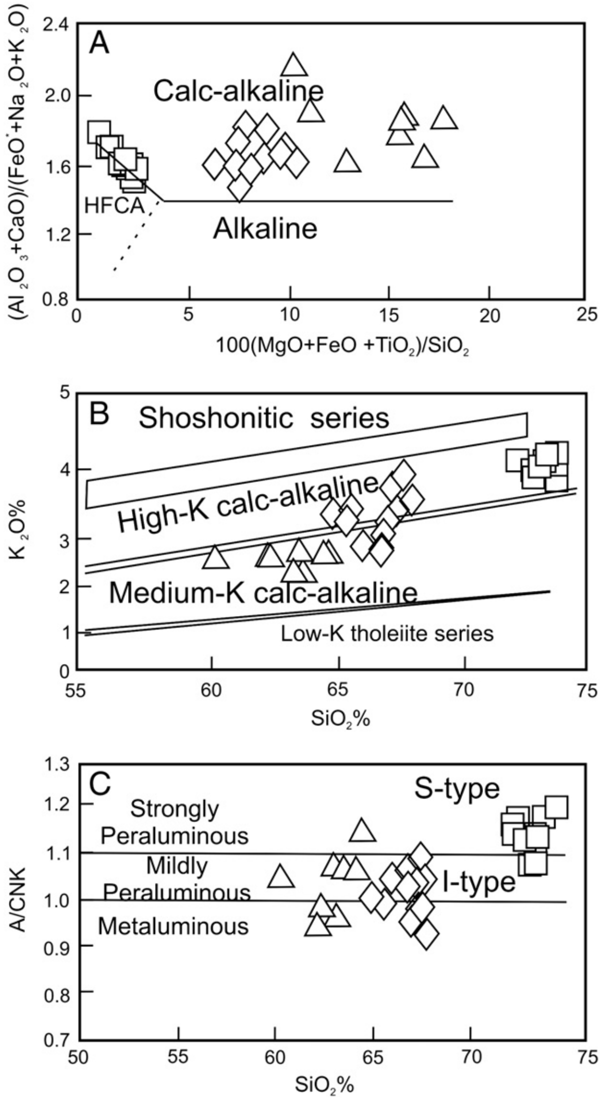

Fig. 4. (A) $(Al_2O_3 + CaO)/(FeO^* + Na_2O + K_2O)$ versus $100(MgO + FeO^* + TiO_2)/SiO_2$ binary plot. (B) K_2O versus SiO_2 binary diagram. Shaded bands are the boundaries between series (Rickwood, 1989). Symbols as in Fig. 2. (C) Molar ratio A/CNK versus SiO_2 binary diagram of Clarke (1992).
Fields of alkaline, calc-alkaline and highly fractionated calc-alkaline (HFCA) line are after Sylvester (1989). Division between I- and S-type granitoids is from Chappell and White (1974).

patterns of the MG rocks show a negative slope, with LILE enrichment, but this trend is significantly obscured by marked anomalies in Ba (Fig. 5B).

Five zircons of the monzogranite MG give a concordia age of 199.8 ± 3.7 Ma with an MSWD of 3.3 (Fig. 6). The relatively large MSWD is the result of large uncertainties in ^{207}Pb measurements, commonly seen in Phanerozoic zircons (e.g., Ireland and Williams, 2003). However, weighted average $^{206}Pb/^{238}U$ age of 200.1 ± 7.2 Ma (2σ) for this sample has a robust MSWD of 0.23 and therefore supports integrity of the concordia age (Table 2). Six of the separated zircons from the granodiorite GD unit yield a concordia age of 212 ± 5.2 Ma (Table 2). Fig. 6 illustrates the concordia plot of these zircons. Weighted average $^{206}Pb/^{238}U$ age for these zircons is 213 ± 11 (2σ) (Table 2). Karimpour et al. (2010a), based on an analysis of 21 points on zircon grains, obtained an age of 217 ± 4–215 ± 4 Ma for the DTG. Karimpour et al. (2010b, 2011) also reported U–Pb zircon for samples from MG and GD as 205.9 ± 4.1 Ma and 201 ± 3.7 Ma, respectively. These ages, however, are not consistent with the cross-cutting relationships because field observations clearly show that MG suite, located in the northern portion of the Mashhad batholith, is cut by the GD unit and thus the former must be younger than the latter.

The whole-rock Rb–Sr and Sm–Nd isotopic data from the studied samples are given in Table 3. Accounting for the 2σ errors on Rb–Sr and Sm–Nd isotope data, the MG differs markedly from the GD by having a higher measured $^{87}Sr/^{86}Sr$ ratio and lower measured $^{143}Nd/^{144}Nd$ ratio and ε_{Nd} values. Considering ages of 217 Ma for the DTG, 212 Ma for the GD and 199.8 Ma for the MG, the calculated initial $^{87}Sr/^{86}Sr$ ratios range 0.708042–0.708368, 0.705469–0.706356 and 0.707457–0.709710, while the initial $^{143}Nd/^{144}Nd$ ratios vary from 0.512044 to 0.512078, from 0.512204 to 0.512225 and from 0.512042 to 0.512111, respectively. In the Nd–Sr isotope diagram (Fig. 7), all the studied granitoid samples plot in the enriched quadrant.

6. Discussion

The geochemistry and mineralogy of the granitoids reflect not only the nature of the protoliths from which these magmas were derived, but also the dynamic conditions under which they were formed, evolved and eventually crystallized out (Altherr et al., 2000). The field relationships, petrology and geochemistry of the granitoid rocks from Mashhad indicate that they had a complex origin, involving distinct parental magmas. The Mashhad granitoids and their surrounding ophiolites and the metamorphic rocks, generated during the subduction and closure of the Paleo-Tethys, are the only mappable units in Iran that can provide clues to the geodynamic history of Paleo-Tethys. Dating by the $^{40}Ar/^{39}Ar$ method on the ophiolites revealed plateau ages of 281.4–277.4 Ma (Ghazi et al., 2001), implying that subduction of the Paleo-Tethys must have occurred after early Permian time. A number of authors (e.g. Davoudzadeh and Schmidt, 1984; Stampfli, 1996; Stampfli and Pillevuit, 1993; Stampfli et al., 1991; Wilmsen et al., 2009; Zanchi et al., 2006) have suggested that the initial closing of Paleo-Tethys started in early Carnian time (c.a. 225 Ma), transforming the northern margin of the Iran Plate into a peripheral foreland basin. This view is reinforced by the paleogeographic history of the Mesozoic foreland–basin complex formed along the northern Iranian micro-continent. During the remainder of the Late Triassic (216–200 Ma), the flexural foreland basin in northern Iran was filled with syn-orogenic siliciclastic sediments and a significant deformation event associated with a distinct increase in sediment supply affected this basin around the Triassic–Jurassic boundary (ca. 200 Ma) (Wilmsen et al., 2009; Zanchi et al., 2011). These processes reflect an increase in relief and erosion, marking the time of collision and coincide with the crystallization of the MG suite from Mashhad. In the Rb vs. Y + Nb diagram (Fig. 8A), the MG analyses lay in the field of syn-collision granitoids, whereas the DTG and GD samples fall in the uppermost corner of the volcanic arc granitoids field. The ~200 Ma MG suite was thus generated during the collision of Iran and Turan paltes, while the DTG and GD suites, formed 12–17 Ma earlier, are interpreted as pre-collisional (subduction-related) granitic bodies. The arc nature of DTG-GD suites supports the hypothesis by Natal'in and Şengör (2005) that the North Pamir–Mashhad arc formed in the southern boundary of the Turan domain (Fig. 1A).

Granitoid rocks can originate from a wide range of petrological sources, from pure mantle to pure crust (upper and lower crust). In the granite classification scheme of Chappell and White (1974, 1992), I-type granites are metaluminous to slightly peraluminous and formed from mantle source or mafic meta-igneous rock components, while S-type granites are inferred to have formed from melting of metasedimentary rocks. Field relations such as the presence of micaceous enclaves, petrographic evidence such as the presence of muscovite, the high-K calc-alkaline peraluminous composition and the presence of corundum in the normative mineralogy all indicate that the MG is an S-type granite (e.g. Barbarin, 1996; Pitcher, 1983). In contrast, the existence of abundant mafic enclaves, the lack of

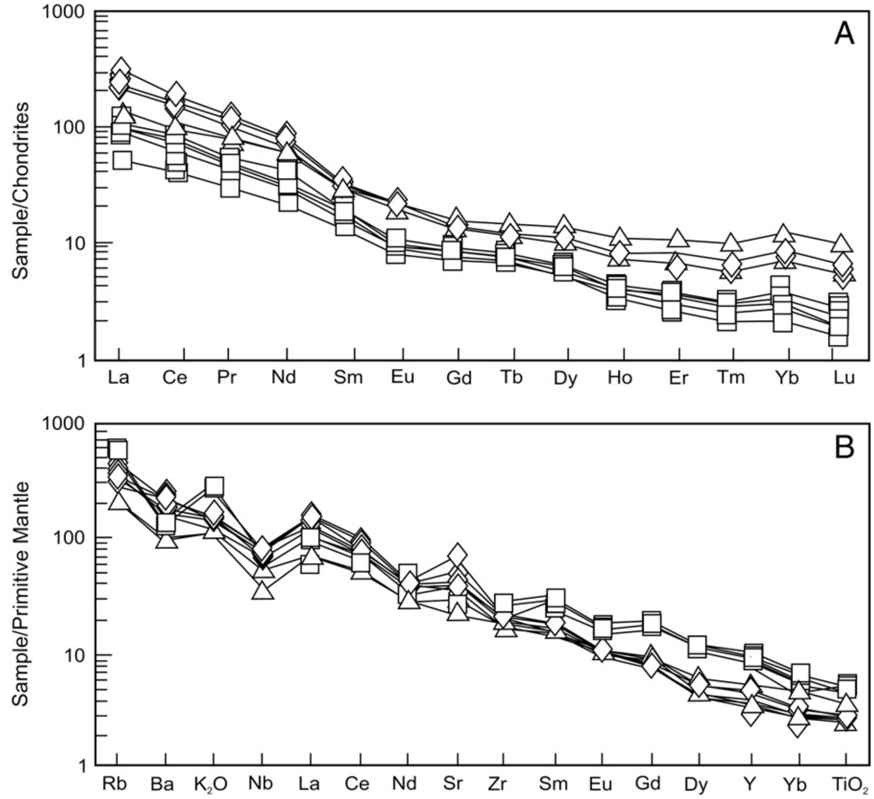

Fig. 5. (A) Chondrite-normalized REE patterns for representative samples of Mashhad granitoid suites. (B) Primitive mantle incompatible trace elements patterns for Mashhad granitoid suites. Symbols as in Fig. 2.
Normalization values in panel A are after Haskin et al. (1968). Normalization values in panel B are after Hofmann (1988).

normative corundum, the metaluminous to slightly peraluminous affinity and the medium-K to high-K calc-alkaline nature (Fig. 4B and C) suggest that DTG and GD both belong to the I-type granites.

The DTG rocks are characterized by significant negative Ba and Nb anomalies and high abundances of LILE (Fig. 5B). They are also enriched in LREE, depleted in HFSE with flat HREE patterns and weakly negative Eu anomalies (Eu/Eu* = 0.67–0.95, Fig. 5A). These geochemical characteristics are usually regarded as signatures of subduction-related and/or crust-derived magmas (Whalen et al., 1996). Three petrogenetic models can be put forward to explain the elemental and isotopic composition of the DTG suite in the Mashhad area. These include (1) fractional crystallization of a basic mantle source, with subsequent modification by assimilation-fractional crystallization (AFC) processes during the ascent to the surface, (2) fractionation of melts produced by anatexis of mafic crustal rocks; and (3) fractionation of mantle-derived mafic melts in a subduction-related environment (e.g. Barbarin, 1999; DePaolo, 1981; Ding et al., 2011; Harris et al., 1986; Jiang et al., 2010; Rapp and Watson, 1995; Roberts and Clemens, 1995; Sisson et al., 2005; Zhang et al., 2007). In the AFC model, the relatively high SiO_2 contents (60–65 wt.%) and low Mg# (0.22–0.36) in the DTG require a significant fractionation of mafic minerals during magma evolution. However, the low Rb/Sr ratios (0.18–0.32) rule out an origin from a mafic magma by extensive fractional crystallization. The small negative (Eu/Eu*)n ratios of the DTG suite (0.67–0.95) are also inconsistent with fractional crystallization of plagioclase from a basaltic parent source (Fig. 5A), because the fractional crystallization of this mineral would yield large negative Eu anomalies (Wilson, 2007). Crustal contamination by SiO_2- and K_2O-rich crust or mixing with a crustally-derived melt during magma ascent would increase the values of K_2O/P_2O5 and K_2O/TiO_2 in magmas (Hooper, 1982). The DTG samples have limited variation of K_2O/P_2O_5 and K_2O/TiO_2 values, inconsistent with evolution by AFC processes. Some geochemical attributes of the DTG suite such as high Cr (8–54 ppm), V (28–78 ppm) contents and Mg# values (0.22–0.36) are found only in the mantle-derived magma and/or in the mafic rocks of lower crust. Experimental studies (Altherr et al., 2000; Rapp and Watson, 1995; Sisson et al., 2005) and theoretical considerations (Roberts and Clemens, 1995) suggest that dehydration-melting of crustal basaltic compositions can produce low silica (<62 wt.% SiO_2) metaluminous mafic melts. However, these mafic melts are mostly marked by low MgO and high Al_2O_3, which are not the case of the studied DTG suite (MgO = 1.32–2.54 wt.%, Al_2O_3 = 14.89–17.45 wt.%, Table 1). Thus, partial melting of a mafic mantle source would appear necessary to account for the major and trace element features of the DTG suite. This source, however, was enriched, possibly during the subduction process, as revealed by the incompatible trace element contents and Sr and Nd isotopic compositions of the DTG samples (Tables 1 and 3). The DTG rocks have high $^{87}Sr/^{86}Sr$ ratios (0.708042–0.708368), low $^{143}Nd/^{144}Nd$ ratios (0.512044–0.512078) and negative $\varepsilon_{Nd(t)}$ values (−5.5 to −6.1) suggesting that their magma was derived from a fractionated mafic mantle melt that has been controlled by sialic crust materials. There is general agreement that many of the highly incompatible large-ion lithophile elements (LILE, e.g. Sr, Rb, Ba, U, Th) and light rare elements in arc magmas are controlled by slab contributions (e.g. Hawkesworth et al., 1993: Murphy, 2007; Pearce and Peate, 1995) and that these elements are released from both sedimentary and igneous layers of the subducting crust (e.g. Elliott et al., 1997; Pearce and Parkinson, 1993; Tollstrup et al., 2010). In this respect, the mantle-derived magma of the arc-related DTG suite is most likely controlled by the subducted sediments and/or oceanic crust during subduction process and their generation above the subducting slab. The Nb/La (0.74 to 0.53) and Nb/Ce (0.36 to 0.26) ratios of the DTG are somewhat closer to average crustal values of 0.69 and 0.33, respectively (Taylor and McLennan, 1985). The average K/Rb value for the DTG samples (236) is closer to those of the upper continental crust ratios of 250 (Taylor and McLennan, 1985). These features

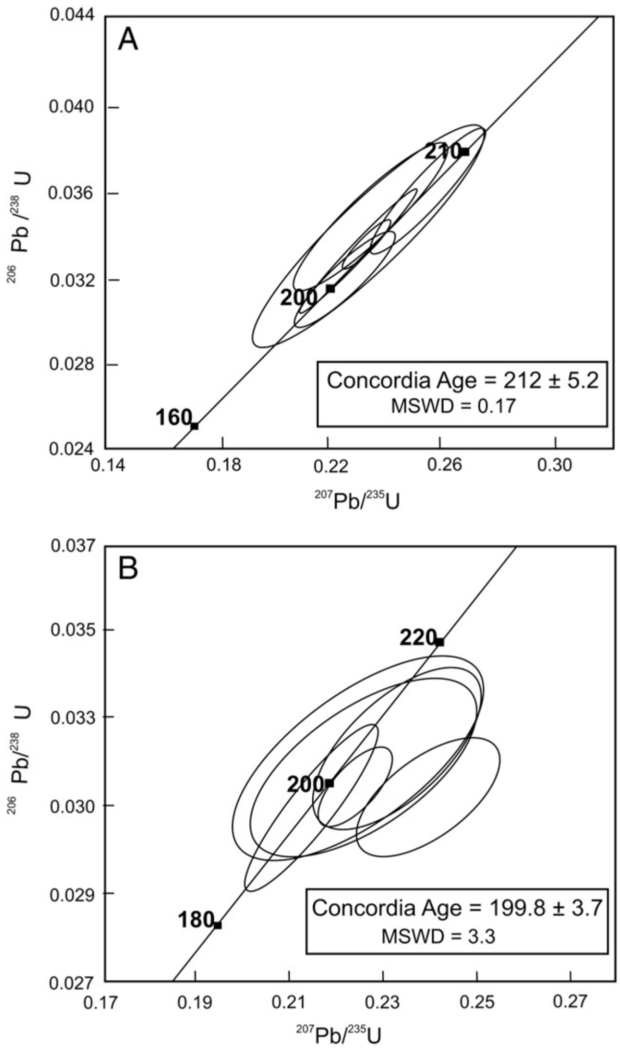

Fig. 6. Zircon U–Pb concordia diagram of (A) the granodiorite suite, and (B) the monzogranite suite of the Mashhad batholith.

assume that the parent magma of the DTG has been controlled by silalic crust materials in the source and/or during magma ascending. Thus, the Dehnow Vakilabad DTG suit is most probably originated by fractional crystallization of a mantle-derived magma that was contaminated by subducted sediments and igneous oceanic crustal materials. The partial melting of subducted slab materials could have been favored by high heat flow during a pre-collision event between the Iran and Turan plates (217–215 ± 4 Ma) during the initial closure of the Paleo-Tethys Ocean. All these geochemical features support the idea that the parental magma of the DTG suite formed during the subduction of Paleo-Tethys oceanic slab in pre-collision zone of Iran and Turan plates.

As to the origin of the Mashhad GD suite, the medium-K calc-alkaline to high-K calc-alkaline and metaluminous to mildly peraluminous nature of these rocks (Fig. 4 B and C) requires a relatively K-rich source(s) (e.g. Roberts and Clemens, 1993). In addition, the GD rocks possess the geochemical signature of adakite magmas (Defant and Drummond, 1990), and fall in the adakite field on the Sr/Y vs. Y diagram (Fig. 8B). The chondrite-normalized REE patterns for the GD samples are strongly fractionated ($(La/Yb)_n > 28$) and do not contain significant Eu-anomalies (Fig. 5A). The enrichment of Sr in the adakitic GD rocks, together with the minor Eu-anomalies indicates that their mantle source was devoid of plagioclase. Also, depletion of Y and Yb requires melting of a source component within the stability field of garnet, most probably under eclogite-facies conditions (Castillo, 2012; Defant and Drummond, 1990). Two possibilities exist for such a garnet-bearing source to generate high Sr/Y and La/Yb melts: (1) partial melting of a delaminated lower crust and reaction of this melt with upwelling astherospheric mantle (e.g. Petford and Atherton, 1996; Wang et al., 2006; Zhang et al., 2007), and (2) partial melting of subducted oceanic slab and interaction of the slab-derived melt with peridotite above the mantle wedge (e.g. Defant and Drummond, 1990; Luo et al., 2002; Tsuchiya et al., 2005; Yogodzinski et al., 2001). The general lack of zircon inheritance in the studied GD samples and coeval Mashhad dakitic GD suite with arc magmas in North Pamir–Mashhad arc (Natal'in and Şengör, 2005) at the southern boundary of the Turan domain are inconsistent with a model involving partial melting of delaminating lower crust. In addition, detailed simulation indicates that the binary mixing curve between depleted mantle and thickened lower crustal rock-derived melts is a convex-up curve (Jiang et al., 2010), which could not account for the observed Sr–Nd isotopic compositions of the GD samples (Fig. 7), and thus argue against the delamination model of thickened lower crust. The primitive mantle-normalized incompatible element patterns of the GD rocks (Fig. 5B) exhibit considerable enrichment in LILEs and a negative Nb anomaly, suggesting an affinity with magmas generated in a subduction-related tectonic setting. Martin et al. (2005) classified adakitic rocks into two groups of high-silica adakites (>60 wt.% SiO_2) and low-silica adakites. The

Table 2
Zircon U–Pb ion-microprobe data of Mashhad granodiorite (GD) and monzogranite (MG) suites, northeastern Iran.

	^{207}Pb*/^{235}U	Error 1σ	^{206}Pb*/^{238}U	Error 1σ	Error corr	^{207}Pb*/^{206}Pb*	Error 1σ	% Radiogenic ^{206}Pb	Age (Ma) ^{206}Pb/^{238}U	Error 1σ	Age (Ma) ^{207}Pb/^{235}U	Error 1σ	Age (Ma) ^{207}Pb/^{206}Pb	Error 1σ
GD suite														
GD1	0.2252	0.0119	0.0320	0.0015	0.95	0.0511	0.0009	99.79	202.8	9.6	206.3	9.8	246.0	39.3
GD2	0.2299	0.0137	0.0333	0.0019	0.98	0.0501	0.0007	99.89	211.0	11.7	210.1	11.3	200.4	30.1
GD3	0.2338	0.0280	0.0341	0.0035	0.95	0.0498	0.0019	98.42	215.9	21.9	213.3	23.1	184.5	90.2
GD4	0.2368	0.0170	0.0348	0.0025	0.98	0.0494	0.0007	99.82	220.5	15.4	215.8	14.0	164.4	35.1
GD9	0.2474	0.0177	0.0352	0.0025	0.97	0.0509	0.0009	99.87	223.3	15.3	224.5	14.4	237.0	40.3
GD11	0.2355	0.0177	0.0350	0.0022	0.87	0.0487	0.0018	96.54	222.0	13.8	214.7	14.5	135.5	87.1
Weighted average ^{206}Pb/^{238}U age: 213 ± 11 [5.0%] 95% conf., MSWD = 0.46, probability = 0.81														
Concordia age: 212 ± 5.2 Ma														
MG suite														
MG6	0.2360	0.0126	0.0309	0.0012	0.77	0.0555	0.0019	99.53	196.0	7.5	215.1	10.4	430.3	75.8
MG3	0.2146	0.0099	0.0310	0.0013	0.87	0.0502	0.0011	99.64	196.9	7.8	197.4	8.2	203.9	52.0
MG2	0.2266	0.0169	0.0318	0.0014	0.57	0.0516	0.0032	99.15	202.0	8.6	207.4	14.0	269.7	140.0
MG4	0.2308	0.0131	0.0321	0.0014	0.73	0.0522	0.0020	99.78	203.5	8.5	210.9	10.8	294.0	89.2
MG1	0.2236	0.0179	0.0322	0.0015	0.75	0.0503	0.0028	99.39	204.5	9.2	204.9	14.9	209.7	128.0
Weighted average ^{206}Pb/^{238}U age: 200.1 ± 7.2 [3.6%] 95% conf., MSWD = 0.23, probability = 0.92														
Concordia age: 199.8 ± 3.7 Ma														

Table 3
Rb–Sr and Sm–Nd isotope compositions of Mashhad granitoid rocks, northeastern Iran.

Mashhad granitoids	Rb/Sr	$^{87}Rb/^{86}Sr$	$^{87}Sr/^{86}Sr$	$(^{87}Sr/^{86}Sr)i$	Sm/Nd	$^{147}Sm/^{144}Nd$	$^{143}Nd/^{144}Nd$	$(^{143}Nd/^{144}Nd)i$	$\varepsilon Nd_{CHUR}(0)$	$\varepsilon Nd_{CHUR}(t)$
Quartz diorite–tonalite–granodiorite (DTG) suite										
VA-1	0.284	0.823	0.710905	0.708368	0.176	0.1061	0.512195	0.512044	−8.6	−6.1
VR	0.210	0.606	0.709889	0.708042	0.182	0.1100	0.512234	0.512078	−7.9	−5.5
Granodiorite (GD) suite										
GH	0.123	0.356	0.706935	0.705861	0.140	0.0845	0.512326	0.512209	−6.1	−3.0
SB	0.270	0.781	0.707824	0.705469	0.140	0.0844	0.512342	0.512225	−5.8	−2.7
SA	0.263	0.761	0.708649	0.706356	0.172	0.1036	0.512361	0.512217	−5.4	−2.9
GM	0.190	0.550	0.707915	0.706258	0.150	0.0904	0.512329	0.512204	−6.0	−3.2
Monzogranite (MG) suite										
BD-1	1.522	4.405	0.720539	0.708025	0.203	0.1222	0.512233	0.512074	−7.9	−6.0
CK	1.528	3.288	0.720013	0.707457	0.218	0.1276	0.512249	0.512082	−7.6	−5.8
KA	1.342	3.904	0.720116	0.709025	0.212	0.1332	0.512216	0.512042	−8.2	−6.6
TR	1.285	3.732	0.720313	0.709710	0.221	0.0904	0.512229	0.512111	−8.0	−5.3

high-silica adakites are slab-derived melts, which interacted with the mantle wedge, whereas the low-silica adakites represent a metasomatized mantle. The GD rocks have SiO_2 content (65–68 wt.%) similar to high-silica adakites, suggesting the involvement of slab-derived melts. In the slab concept, the subducted oceanic sediments mainly contribute a generic subduction component consisting mainly of hydrous fluids that interact with the mantle as well as lower the melting temperature of the mantle wedge to generate geochemical characteristics of adakite magma (Castillo, 2012; Shimoda, 2009). In this respect, the high Sr (594–1234 ppm) and Cr (up to 100 ppm) contents and high Nd/Yb ratios (29.73–39.54) of these rocks are also consistent with geochemical features of adakites that originated from subducted slab melts hybridized with peridotite mantle (Yogodzinski and Kelemen, 1998). The GD suite also shows low Y and Yb concentrations (Tables 1 and 2). Such a feature is interpreted to reflect a slab-melt signature in the mantle source (e.g. Martin et al., 2005; Moyen, 2009). Therefore, we suggest that the GD suite of Mashhad batholith was most likely formed by the interaction of slab partial melts with peridotite mantle during ascent in the mantle wedge.

The compositional gap (69–72%) observed between the MG and GD-DTG rocks suggests that these two groups (i.e., MG vs. GD + DTG) did not evolve from the same magma by fractional crystallization. On the Al_2O_3/TiO_2 (ratio %) versus CaO (wt.%) diagram, the MG samples have significantly higher Al_2O_3/TiO_2 values (>50) and considerably lower CaO (<1.5%) contents relative to those of the DTG-GD samples (Fig. 9A). In addition, the MG suite has higher Rb/Nb values (>8) with noticeably restricted Na_2O/K_2O ratios (0.6–0.8) on the binary Rb/Nb–Na_2O/K_2O diagram (Fig. 9B). These geochemical attributes suggest that the MG evolved from a distinct source relative to the DTG and GD. The MG suite of the Mashhad batholith is mildly peraluminous to strongly peraluminous, with A/CNK values ranging from 1.07 to 1.17 (Fig. 4C), indicating a transition from I- to S-type and high-K calc-alkaline nature. This suite also shows relatively low CaO (0.83–1.31 wt.%) and Sr (<250 ppm) content, plus slightly negative Eu-anomalies (Fig. 5A), and low Sr/Ba ratio (0.35–0.67), which require melting of a source rock within the stability field of plagioclase (Barnes et al., 1996; Martin, 1999). Also, the relatively low HREE (Yb ≤ 1 ppm) and Y (≤20 ppm) contents as well as the

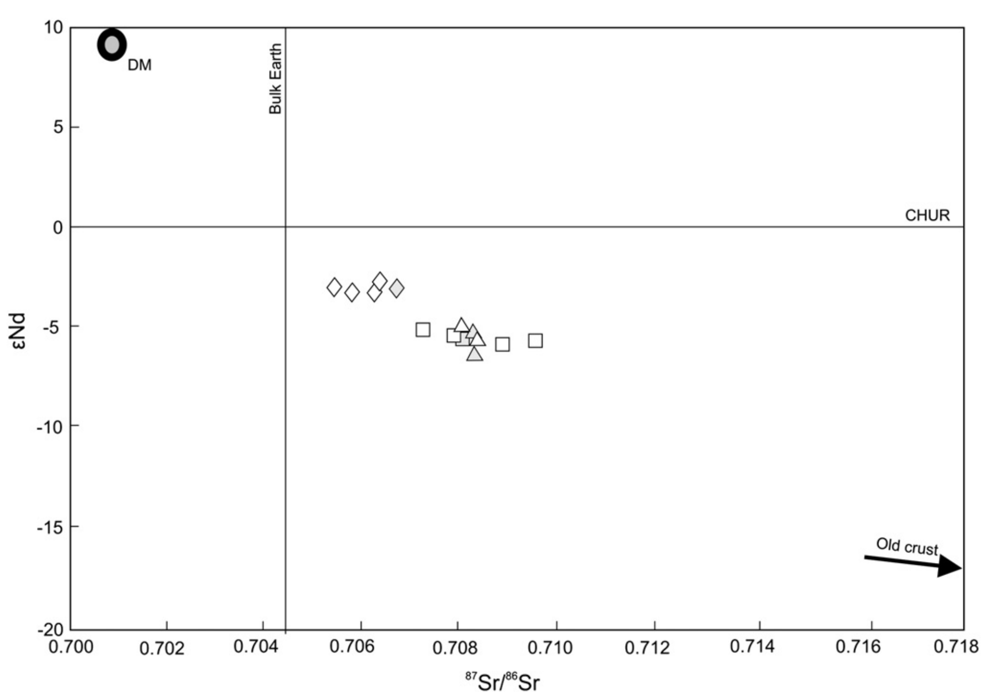

Fig. 7. ε_{Nd} vs $^{87}Sr/^{86}Sr$ for the granites from Mashhad. DM = depleted mantle and CHUR = chondrite uniform reservoir. Symbols as in Fig. 2. The field of old crust is based on the Sr and Nd isotope analyses of a metamorphosed shale that surrounds Mashhad batholith (Karimpour et al., 2010a).
Filled symbols represent Sr and Nd isotope data for Mashhad granitoids, reported by Karimpour et al. (2010a, 2010b, 2011).

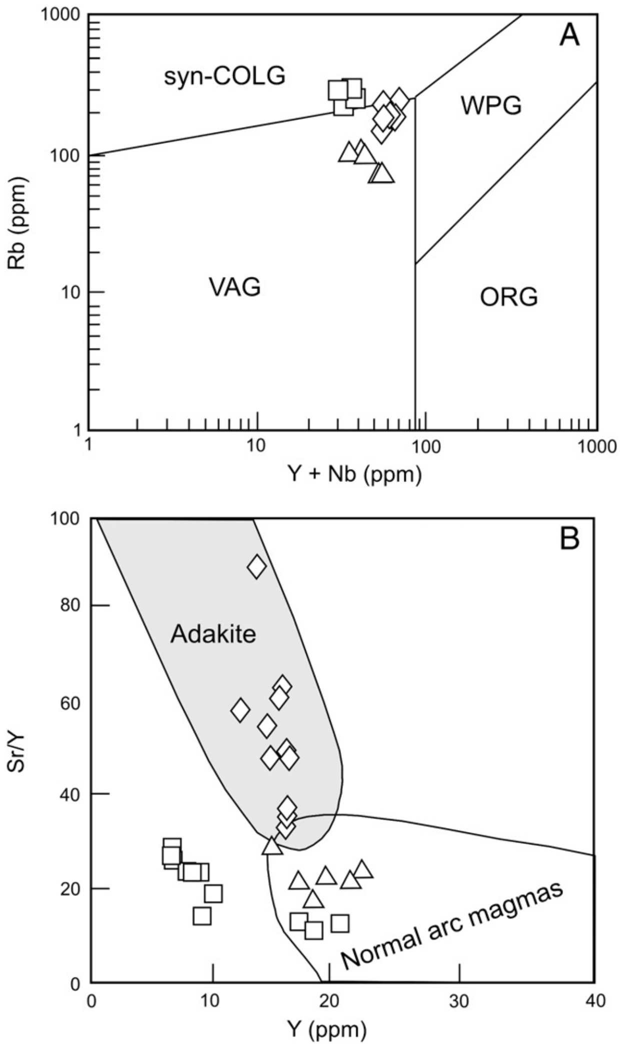

Fig. 8. (A) Discrimination diagram of Rb versus Y + Nb. VAG = volcanic arc granites; syn-COLG = syn-collision zone granitoids; ORG = ocean ridge granites; and WPG = within-plate granites. (B) Sr/Y vs. Y diagram binary diagram for the Mashhad granitoid suites. Symbols as in Fig. 2.
Fields in panel A are after Pearce (1996). Panel B is after Defant and Drummond (1990).

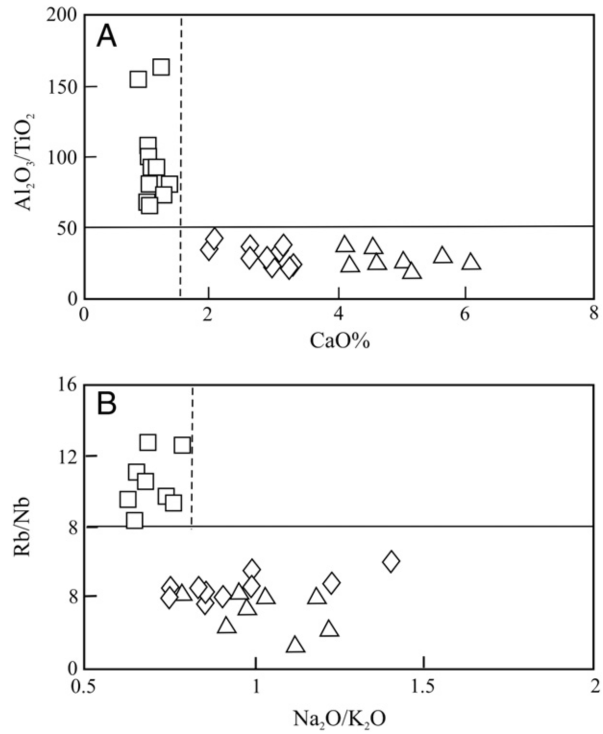

Fig. 9. (A) % Al_2O_3/TiO_2–wt.% CaO relationships for the studied granitoids of the Mashhad region. (B) Rb/Nb against %Na_2O/K_2O for the studied granitoid rocks of the Mashhad area. Symbols as in Fig. 2.

steep HREE patterns (Fig. 5A) suggest that garnet, rather than amphibole, was a residual phase in the source of the MG rocks. These geochemical features were originally related to partial melting of subducted oceanic crust (Defant and Drummond, 1990), but there is increasing evidence that melting of metasedimentary materials in the lower crust can explain such trace-element characteristics (Gao et al., 2004; Rapp et al., 1999; Xu et al., 2002; Wan et al., 2009). The peraluminous nature of the MG requires a peraluminous protolith such as a metasedimentary assemblage. High pressure–temperature experiments show that during the dehydration-melting of metasedimentary rocks (biotite gneiss), garnet is present as one of residual phases at pressures ≥12.5 kbar and plagioclase remains stable up to 15 kbar (Patiño-Douce and Beard, 1995). The fact that both garnet and plagioclase are residual phases in the source of MG suite implies that the source region is relatively deep lower crust (~40–50 km, corresponding to 12.5–15 kbar). The geochemical characteristics of the MG suite, including low initial $^{143}Nd/^{144}Nd$ ratios (0.512042–0.512111), high initial $^{87}Sr/^{86}Sr$ ratios (0.707457–0.709710), and $\varepsilon_{Nd(t)}$ values (−5.3 to −6.0), thus suggest that it was generated by partial melting of metasedimentary rocks in the thickened lower continental crust during a collisional event related to the closure of the Paleo-Tethys Ocean.

Based on the above observations, the differences in the composition of the studied granitoids from the Mashhad area are the result of the geodynamic evolution of the Turan–Iran Plate through a subduction to collisional setting. This is consistent with the previously published data from other parts of the Silk Road arc. Jiang et al. (2010) classified the granitiods from the Qinling orogen in central China into the Carnian (227–218 Ma) and Norian (211 Ma) plutons, and suggested that the Carnian plutons were emplaced in a continental arc setting while the Norian pluton was emplaced during continental collision between the South Qinling terrane and South China. Based on the detailed study of Karakoram Range (SE Pamir), Zanchi and Gaentani (2011) attributed the deformation of metabasites and gneiss in the Trich boundary zone to the collision of Karakoram with East Hindu Kush at the end of Triassic or beginning of the Jurassic. Studies from north Pamir also point to the Cimmerian orogeny that resulted from the late Triassic–early Jurassic closure of the Paleo-Tethys (Schwab et al., 2004). In Turkey, the subduction of Paleo-Tethys continued till the medial Jurassic by the arrival of the Turkish/Tavric units of Gondwanan origin (Natal'in and Şengör, 2005). The subduction and collision history of Paleo-Tethys in Mashhad area that is inferred from the study of granitoids, corresponds well to the history of Cimmerian orogeny in other parts of Silk Road arc.

7. Conclusions

Granitic rocks exposed in the vicinity of Mashhad City, in northeastern Iran can be classified into: (1) medium-K calc-alkaline metaluminous to peraluminous quartz diorite, tonalite and granodiorite (DTG), (2) medium- to high-K calc-alkaline metaluminous granodiorite (GD) and (3) high-K calc-alkaline mildly peraluminous to strongly peraluminous monzogranite (MG). They demonstrate co-existing I- and S-type granitoids formed during subduction of Paleo-Tethys and the final collision of the Iran micro-continent with Eurasia. The petrologic and geochemical properties of the DTG and GD suites are typical of I-type granites emplaced in an arc regime during the subduction of the Paleo-Tethys Ocean under the Turan Plate. They are enriched in LREE, depleted in HFSE with flat HREE patterns, have weakly negative Eu anomalies and show negative primitive-mantle normalized Nb anomalies, low $\varepsilon_{Nd(t)}$ values (−2.7 to −6.1), low initial $^{143}Nd/^{144}Nd$ ratios (0.512014–0.512225) and high initial $^{87}Sr/^{86}Sr$ values (0.705469–0.708368), indicative of mantle-derived granites. The DTG suite (217–215 Ma) was produced by fractional crystallization of mantle-derived magma that was controlled by subduction components of the pre-collision zone between the Iran and the Turan plates. The GD rocks (212 Ma) have the geochemical characteristics of adakitic magmas, generated by partial melting of a subducted slab that also interacted with the mantle wedge peridotites. The MG is a two-mica granite and can be classified as a peraluminous leucocratic granite. The geochemical characteristics of the MG suite, including low initial $^{143}Nd/^{144}Nd$ ratios (0.512042–0.512111), high initial $^{87}Sr/^{86}Sr$ ratios (0.707457–0.709710), and $\varepsilon_{Nd(t)}$ values (−5.3 to −6.6), suggest that it was generated by dehydration melting of a heterogeneous Al-rich metasedimentary assemblage from the lower continental crust. The MG (200 Ma) was produced the consequence of a collisional event, related to the closing of the Paleo-Tethys Ocean. The ages of Mashhad granites show that subduction of Paleo-Tethys Ocean crust which occurred after Permian, resulted in the collision of the Iran micro-continent and Eurasia in Early Jurassic.

Acknowledgment

This paper is dedicated to the memory of Prof. André E. Lalonde, who contributed greatly to this paper. The analytical assistance from Axel Schmitt of the Keck ion microprobe facility, University of California, Los Angeles (UCLA) is acknowledged. The ion microprobe facility at UCLA was partly supported by a grant from the Instrumentation and Facilities Program, Division of Earth Sciences, National Science Foundation. Nasrin Rashid Moghaddam and Ramin Samadi provided samples for U–Pb dating. The manuscript has been improved by the constructive criticisms of the two anonymous reviewers. We thank Prof. Nelson Eby (Editor-in-chief) for his thoughtful review and constructive comments.

Appendix A. Supplementary data

Supplementary data to this article can be found online at http://dx.doi.org/10.1016/j.lithos.2013.03.003.

References

Alavi, M., 1979. The Virani ophiolite complex and surrounding rocks. Geologische Rundschau 68, 334–341.
Alavi, M., 1991. Sedimentary and structural characteristics of the Paleo-Tethys remnants in northeastern Iran. Geological Society of America Bulletin 1038, 983–992.
Alberti, A., Nicoletti, M., Petrucciani, C., 1973. K–Ar ages of micas of Mashhad granites. Periodico di Mineralogica 423, 483–493.
Alsharhan, A.S., Rizk, Z.A., Narin, A.E., Bakhit, D.W., Alhajri, S.A., 2001. Hydrogeology of an Arid Region: The Arabian Gulf and Adjoining Areas. Elsevier Science, Amsterdam 205–230.
Altherr, R., Holl, A., Hegner, E., Langer, C., Kreuzer, H., 2000. High-potassium, calc-alkaline plutonism in the European Variscides: northern Vosges (France) and northern Schwarzwald (Germany). Lithos 50, 51–73.
Barbarin, B., 1996. Genesis of the two main types of peraluminous granitoids. Geology 24, 295–298.
Barbarin, B., 1999. A review of the relationships between granitoid types, their origins and their geodynamic environments. Lithos 46, 605–626.
Barnes, C.G., Petersen, S.W., Kistler, R.W., Murray, R., Kays, M.A., 1996. Source and tectonic implications of tonalite–trondhjemite magmatism in the Klamath Mountains. Contributions to Mineralogy and Petrology 123, 40–60.
Berberian, M., King, G.C., 1981. Towards a paleogeography and tectonic evolution of Iran. Canadian Journal of Earth Sciences 1811, 1764–1766.
Castillo, P.R., 2012. Adakite petrogenesis. Lithos 134–135, 304–316.
Chappell, B.W., White, A.J.R., 1974. Two contrasting granite types. Pacific Geology 8, 173–174.
Chappell, B.W., White, A.J.R., 1992. I- and S-type granites in the Lachlan Fold Belt. Transactions of the Royal Society of Edinburg, Earth Sciences 83, 1–26.
Clarke, D.B., 1992. Granitoid Rocks. Chapman and Hall, London (238 pp.).
Compston, W., Williams, I.S., Meyer, C., 1984. U–Pb geochronology of zircons from lunar breccia 73217 using a sensitive high mass-resolution ion microprobe. Journal of Geophysical Research 89, B525–B534.
Cousens, B.L., Clague, D.A., Sharp, W.D., 2003. Chronology, chemistry and origin of trachytes from Hualalai volcano, Hawaii. Geochemistry, Geophysics, Geosystems 4, 1–27.
Davoudzadeh, M., Schmidt, K., 1984. Plate tectonics, orogeny, and mineralization in the Iranian fold belts; report of a German–Iranian research program 1977–1978. Neues Jahrbuch fuer Geologie und Palaeontologie Abhandlungen 168, 182–207.
Defant, M.J., Drummond, M.S., 1990. Derivation of some modern arc magmas by melting of young subducted lithosphere. Nature 347, 662–665.
DePaolo, D.J., 1981. Trace element and isotopic effects of combined wallrock assimilation and fractional crystallization. Earth and Planetary Science Letters 53, 189–202.
Ding, L.X., Ma, C.Q., Li, J.-W., Robinson, P.T., Deng, X.D., Zhang, C., Xu, W.C., 2011. Timing and genesis of the adakitic and shoshonitic intrusions in the Laoniushan complex, southern margin of the North China Craton: implications for post-collisional magmatism associated with the Qinling Orogen. Lithos 126, 212–232.
Elliott, T., Plank, T., Zindler, A., White, W., Bourdon, B., 1997. Element transport from subducted slab to juvenile crust at the Mariana arc. Journal of Geophysical Research 102, 14991–15019.
Gao, S., Rudnick, R.L., Yuan, H.L., Liu, X.M., Liu, Y.S., Xu, W.L., Ling, W.L., Ayers, J., Wang, X.C., Wang, Q.H., 2004. Recycling lower continental crust in the North China Carton. Nature 432, 892–897.
Ghazi, M., Hassanipak, A.A., Tucker, P.J., Mobasher, K., 2001. Geochemistry and $^{40}Ar–^{39}Ar$ ages of the Mashhad Ophiolite, NE Iran. Eos Transactions. American Geophysical Union, Fall Meeting, 82 (47).
Harris, N.B.W., Pearce, J.A., Tindle, A.G., 1986. Geochemical characteristics of collision-zone magmatism. Geological Society of London, Special Publication 19, 67–81.
Hashemi, S.F., 2004. Petrology and depositional environment of Jurassic conglomerate in southern Mashhad. Unpublished M.Sc. Thesis, Geology Department, Ferdowsi University of Mashhad 199p.
Haskin, L.A., Haskin, M.A., Frey, F.A., Wildemann, T.R., 1968. Relative and absolute terrestrial abundances of the rare earths. In: Ahrens, L.H. (Ed.), Origin and Distribution of Elements. Pergamon Press, New York, pp. 889–912.
Hawkesworth, D.J., Gallagher, K., Hergt, J.M., McDermott, F., 1993. Mantle and slab contributions in arc magmas. Annual Review of Earth and Planetary Sciences 21, 175–204.
Hofmann, A.W., 1988. Chemical differentiation of the Earth: the relationship between mantle continental crust and oceanic crust. Earth and Planetary Science Letters 90, 297–314.
Hooper, P.R., 1982. The Columbia River basalts. Science 215, 1463–1468.
Ireland, T.R., Williams, I.S., 2003. Considerations in zircon geochronology by SIMS. In: Manchar, J.M., Hoskin, P.W.O. (Eds.), Zircon: Reviews in Mineralogy and Geochemistry, 53, pp. 215–241.
Jiang, Y.-H., Jin, G.-D., Liao, S.-Y., Zhou, Q., Zhao, P., 2010. Geochemical and Sr–Nd–Hf isotopic constraints on the origin of Late Triassic granitoids from the Qinling orogen, central China: implications for a continental arc to continent–continent collision. Lithos 117, 183–197.
Karimpour, M.H., Stern, C.R., Farmer, L., 2010a. Zircon U–Pb geochronology, Sr–Nd isotope analyses, and petrogenetic study of the Dehnow diorite and Kuhsangi granodiorite (Paleo-Tethys), NE Iran. Journal of Asian Earth Sciences 37, 384–393.
Karimpour, M.H., Stern, C.R., Farmer, L., 2010b. Geochronology, radiogenic isotope geochemistry, and petrogenesis of Sangbast Paleo-Tethys monzogranite, Mashhad, Iran. Iranian Journal of Crystallography and Mineralogy 17, 706–719.
Karimpour, M.H., Stern, C.R., Farmer, L., 2011. Rb–Sr and Sm–Nd isotopic compositions, U–Pb age and petrogenesis of Khajeh Mourad Paleo-Tethys leucogranite, Mashhad, Iran. Geosciences: Quaternary Journal of the Geological Survey of Iran 20, 171–182 (In Farsi).
Ludwig, K.R., 2003. Isoplot 3.0. A geochronological toolkit for Microsoft Excel. Berkeley Geochronology Center Special Publication No. 4. (70 pp.).
Majidi, B., 1978. Étude pétrostructurale de la région de Mashhad (Iran). Les problèmes des métamorphites, serpentinites et granitoïdes hercyniens. Thèse de l'Université Scientifique et Médicale de Grenoble, France.
Luo, Z.H., Ke, S., Cao, Y.Q., Deng, J.F., Chen, H.W., 2002. Late Indosinian mantle-derived magmatism in the East Kunlun. Geological Bulletin of China 21, 292–297.
Martin, H., 1999. Adakitic magmas: modern analogues of Archaean granitoids. Lithos 46, 411–429.
Martin, H., Smithies, R.H., Rapp, R., Moyen, J.-F., Champion, D., 2005. An overview of adakite, tonalite–trondhjemite–granodiorite (TTG), and sanukitoid: relationships and some implications for crustal evolution. Lithos 79, 1–24.
Moyen, J., 2009. High Sr/Y and La/Yb ratios: the meaning of the "adakitic signature". Lithos 112, 556–574.
Murphy, J.B., 2007. Igneous rock associations 8. Arc magmatism II: geo-chemical and isotopic characteristics. Geoscience Canada. Series 34 (1), 7–35.
Natal'in, B.A., Şengör, A.M.C., 2005. Late Palaeozoic to Triassic evolution of the Turan and Scythian platforms: the pre-history of the Paleo-Tethyan closure. Tectonophysics 404, 175–202.
Paces, J.B., Miller, J.D., 1993. Precise U-Pb ages of Duluth Complex and related mafic intrusions, northeastern Minnesota; geochronological insights to physical, petrogenetic, paleomagnetic, and tectonomagnetic processes associated with the 1.1 Ga Midcontinent Rift System. Journal of Geophysical Research 98, 13997–14013.
Patiño-Douce, A.E., Beard, J.S., 1995. Dehydration-melting of biotite gneiss and quartz amphibolite from 3 to 15 kbar. Journal of Petrology 36, 707–738.
Pearce, J.A., 1996. Source and settings of granitic rocks. Episodes 9, 120–125.
Pearce, J.A., Parkinson, I.J., 1993. Trace element models for mantle melting: application to volcanic arc petrogenesis. Geological Society of London, Special Publication 76, 373–403.

Pearce, J.A., Peate, D.W., 1995. Tectonic implications of the composition of volcanic arc magmas. Annual Review of Earth Science Letters 23, 251–285.

Petford, N., Atherton, M.P., 1996. Na-rich partial melts from newly underplated basaltic crust: The Cordillera Blanca batholith, Peru. Journal of Petrology 37, 1491–1521.

Pitcher, W.S., 1983. Granite: typology, geological environment and melting relationships. In: Atherton, M.P., Gribble, C.D. (Eds.), Migmatites, Melting and Metamorphism. Shiva Ltd., Cheshire, pp. 277–285.

Quidelleur, X., Grove, M., Lovera, O.M., Harrison, T.M., Yin, A., Ryerson, F.J., 1997. Thermal evolution and slip history of the Renbu Zedong thrust, southeastern Tibet. Journal of Geophysical Research 102, 2659–2679.

Rapp, R.P., Watson, E.B., 1995. Dehydration melting of metabasalt at 8–32 kbar: implications for continental growth and crust–mantle recycling. Journal of Petrology 36, 891–931.

Rapp, R.P., Shimizu, N., Norman, M.D., Applegate, G.S., 1999. Reaction between slab-derived melts and peridotite in the mantle wedge: experimental constraints at 3.8 GPa. Chemical Geology 727 (160), 335–356.

Razavi, M.H., Masoudi, F., Alaminia, Z., 2008. Garnet–biotite chemistry for thermometry of staurolite schist from south of Mashhad, NE Iran. Journal of Sciences, Islamic Republic of Iran 19, 237–245.

Rickwood, P.C., 1989. Boundary lines within petrologic diagrams which use oxides of major and minor elements. Lithos 22, 247–263.

Roberts, M.P., Clemens, J.D., 1993. Origin of high-potassium, calc-alkaline, I-type granitoids. Geology 21, 825–828.

Roberts, M.P., Clemens, J.D., 1995. Feasibility of AFC models for the petrogenesis of calc-alkaline magma series. Contributions to Mineralogy and Petrology 121, 139–147.

Sañudo-Wilhelmy, S.A., Flegal, A.R., 1994. Temporal variations in lead concentrations and isotopic composition in the Southern California Bight. Geochimica et Cosmochimica Acta 58, 3315–3320.

Schmitt, A.K., Grove, M., Harrison, T.M., Lovera, O.M., Hulen, J., Waters, M., 2003a. The Geysers–Cobb Mountain Magma System, California (Part 1. U–Pb zircon ages of volcanic rocks, conditions of zircon crystallization and magma residence times. Geochimica et Cosmochimica Acta 67, 3423–3442.

Schmitt, A.K., Grove, M., Harrison, T.M., Lovera, O.M., Hulen, J., Waters, M., 2003b. The Geysers–Cobb Mountain Magma System, California (Part 2. Timescales of pluton emplacement and implications for its thermal history). Geochimica et Cosmochimica Acta 67, 3443–3458.

Schwab, M., Ratschbacher, L., Siebel, W., McWilliams, M., Minaev, V., Lutkov, V., Chen, F., Stanek, K., Nelson, B., Frisch, W., Wooden, J.L., 2004. Assembly of the Pamirs: age and origin of magmatic belts from the southern Tien Shan to the southern Pamirs and their relation to Tibet. Tectonics. http://dx.doi.org/10.1029/2003TC001583.

Şengör, A.M.C., 1987. Cross-faults and differential stretching of hanging walls in regions of low-angle normal faulting: examples from western Turkey. In: Coward, M.P., Dewey, J.F., Hancock, P.L. (Eds.), Continental Extensional Tectonics: Geological Society Special Publication, 28, pp. 575–589.

Shimoda, G., 2009. Genetic link between EMI and EMII: an adakite connection. Lithos 112, 591–602.

Sisson, T.W., Ratajeski, K., Hankins, W.B., Glazner, A.F., 2005. Voluminous granitic magmas from common basaltic sources. Contributions to Mineralogy and Petrology 148, 635–661.

Stacey, J.S., Kramers, J.D., 1975. Approximation of terrestrial lead isotope evolution by a two stage model. Earth and Planetary Science Letters 26, 207–221.

Stampfli, G.M., 1996. The Intra-Alpine terrain: a Paleo-Tethyan remnant in the Alpine Variscides. Eclogae Geologicae Helvetiae 89, 13–42.

Stampfli, G.M., Pillevuit, A., 1993. An alternative Permo-Triassic reconstruction of the kinematics of the Tethyan realm. In: Dercourt, J., Ricou, L.-E., Vrielinck, B. (Eds.), Atlas Tethys Palaeoenvironmental Maps, Explanatory Notes. Gauthier-Villars, Paris, pp. 55–62.

Stampfli, G.M., Marcoux, J., Baud, A., 1991. Tethyan margins in space and time. In: Channell, J.E.T., Winterer, E.L., Jansa, L.F. (Eds.), Paleogeography and Paleoceanography of Tethys: Palaeogeography, Palaeoclimatology, Palaeoecology, 87, pp. 373–410.

Stöcklin, J., 1974. Possible ancient continental margins in Iran. In: Burk, C.A., Drake, C.L. (Eds.), The Geology of Continental Margins, pp. 873–887.

Streckeisen, A., Le Maitre, R.W., 1979. A chemical approximation to the modal QAPF classification of the igneous rocks. Neues Jahrbuch für Mineralogie Abhandlungen 136, 169–206.

Sylvester, P.J., 1989. Post-collisional strongly peraluminous granites. Journal of Geology 97, 261–280.

Taylor, S.R., McLennan, S.M., 1985. The Continental Crust: Its Composition and Evolution. Blackwell, Oxford (312 pp.).

Tollstrup, D., Gill, J.B., Kent, A.J.R., Prinkey, D., Williams, R., Tamura, Y., Ishizuka, O., 2010. Across-arc geochemical trends in the Izu–Bonin arc: contributions from the subducting slab, revisited. Geochemistry Geophysics and Geosystem 11 (2009GC002847).

Tsuchiya, N., Suzuki, S., Kimura, J.-I., Kagami, H., 2005. Evidence for slab melt/mantle reaction: petrogenesis of Early Cretaceous and Eocene high-Mg andesites from the Kitakami Mountains, Japan. Lithos 79, 179–206.

Wan, Y.S., Liu, D.Y., Wang, S.Y., Zhao, X., Dong, C.Y., Zhou, H.Y., Yin, X.Y., Yang, C.Q., Gao, L.Z., 2009. Early Precambrian crustal evolution in the Dengfeng area, Henan province (eastern China): constraints from geochemistry and SHRIMP U–Pb zircon dating. Acta Geologica Sinica 7 (83), 982–999.

Wang, Q., Xu, J.F., Jian, P., Bao, Z.W., Zhao, Z.H., Li, C.F., Xiong, X.L., Ma, J.L., 2006. Petrogenesis of adakitic porphyries in an extentional tectonic setting, Dexing, South China: implications for the genesis of porphyry copper mineralization. Journal of Petrology 47, 119–144.

Whalen, J.B., Jenner, J.A., Longstaffe, F.J., Robert, F., Cariepy, C., 1996. Geochemical and isotopic (O, Nd, Pb and Sr) constraints on A-type granite petrogenesis based on the Topsails igneous suites, Newfoundland Appalachians. Journal of Petrology 37, 1463–1489.

Wilmsen, M., Fürsich, F., Seyed-Emmani, K., Majidifard, M.R., Taheri, J., 2009. The Cimmerian Orogeny in northern Iran/tectono-stratigraphic evidence in the foreland. Terra Nova 21, 211–218.

Wilson, M., 2007. Igneous Petrogenesis. Chapman and Hall, London (485 pp.).

Xu, J.F., Shinjio, R., Defant, M.J., Wang, Q., Rapp, R.P., 2002. Origin of Mesozoic adakitic intrusive rocks in the Ningzhen area of east China: partial melting of delaminated lower continental crust. Geology 12, 1111–1114.

Yogodzinski, G.M., Kelemen, P.B., 1998. Slab melting in the Aleutians: implication of an ion probe study of clinopyroxene in primitive adakite and basalt. Earth and Planetary Science Letters 158, 53–65.

Yogodzinski, G.M., Lees, J.M., Churikova, T.G., Dorendorf, F., Woerner, G., Volynets, O.N., 2001. Geochemical evidence for the melting of subducting oceanic lithosphere at plate edges. Nature 409, 500–504.

Zanchi, A., Gaentani, M., 2011. The geology of the Karakoram range, Pakistan: the new 1:100,000 geological map of Central-Western Karakoram. Italian Journal of Geosciences. http://dx.doi.org/10.3301/IJG.

Zanchi, A., Zanchetta, S., Balini, M., Garzanti, E., Nicora, A., Poli, S., Naimi, N., Hosayum, M., 2006. The Paleotethys collision zone in north eastern Iran. Geophysical Research Abstracts 8, 03439.

Zanchi, A., Berra, F., Balini, M., Ghassemi, M.R., Heidarzadeh, G., Zanchetta, S., 2011. The Palaeotethys suture zone in NE Iran: new constraints on the evolution of the Eo–Cimmerian Belt (Darius Programme). AAPG International Conference and Exhibition, Milan, Italy Search and Discovery Article #30222.

Zen, E., 1986. Aluminum enrichment in silicate melts by fractional crystallization: some mineralogic and petrographic constraints. Journal of Petrology 27, 1095–1117.

Zhang, H.F., Parrish, R., Zhang, L., Xu, W.C., Yuan, H.L., Gao, S., Crowley, Q.G., 2007. A-type granite and adakitic magmatism association in Songpan–Garze fold belt, eastern Tibetan Plateau: Implication for lithospheric delamination. Lithos 97, 323–335.